SCITEC186

ELSEVIER

Science and Technology of Advanced Materials 00 (2002) 000–000

SCIENCE AND TECHNOLOGY OF ADVANCED MATERIALS

www.elsevier.com/locate/stam

Design and fabrication of functionally graded PZT/Pt piezoelectric bimorph actuator

Kenta Takagi[a], Jing-Feng Li[b,*], Shohei Yokoyama[a], Ryuzo Watanabe[b], Abdulhakim Almajid[c], Minoru Taya[c]

[a]*Graduate School of Engineering, Tohoku University, Sendai 980-8579, Japan*
[b]*Department of Materials Processing, School of Engineering, Tohoku University, Aoba-yama 02, Sendai 980-8579, Japan*
[c]*Department of Mechanical Engineering, University of Washington, Seattle, WA 98195-2600, USA*

Received 30 November 2001; revised 4 January 2002; accepted 17 January 2002

Abstract

A laminated piezoelectric bimorph actuator with a graded compositional distribution of PZT and Pt was fabricated, and its deflection characteristics were evaluated. Using experimentally determined compositional dependency of elastic and piezoelectric properties in the PZT/Pt composites, the modified classical lamination theory and the finite element method were applied to find the optimum compositional profile that will give a larger deflection and smaller stress, simultaneously. The miniature bimorph-type graded actuator that consists of a composite internal-electrode (PZT/30 vol% Pt) and three piezoelectric layers of different compositions (PZT/0–20 vol% Pt) were fabricated by powder stacking and sintering. The deflection of the actuator was measured using electric strain gages mounted on the top and bottom surfaces of the actuator. The deflection was found to strongly depend on the composition distribution profile. Under an applied electric field of 100 V m^{-1}, the actuator with an optimum composition profile exhibited a curvature of up to 0.03 m^{-1}, which is a satisfactory performance for this kind of actuators. The stress generated on actuation was estimated to be as low as 0.4 MPa, which is much smaller than those of conventional directly bonded actuators and will assure a long actuation life.

Keywords: Piezoelectric actuator; Lead zirconate titanate; Platinum; Functionally graded material; Stress minimization; Classical lamination theory; Finite element method

1. Introduction

Piezoelectric actuators and sensors have novel applications for microelectromechanical system (MEMS) [1,2] and smart material systems, especially in the medical and aerospace industry [3]. A piezoelectric bimorph is a bending-displacement-type of actuator, in which two piezoelectric ceramic plates are stuck together using an adhesive. A positive electric field is applied to the top plate, and a negative electric field, to the bottom one. Under the applied electric field, the top layer extends while the bottom layer shrinks, and this produces a bending deflection. However, high stress is usually generated at the interface due to a large strain difference between the top and bottom layers, which will cause a premature failure at the interface that is bonded with organic adhesive. A spontaneous degradation of the bonding agent also enhances fatigue proneness of this kind of actuators. The reduction of such stress is of first concern for the preparation of long-life bimorph actuators. It is very likely that we can reduce the stress concentration by introducing a compositionally graded layer between two piezoelectric plates, as first proposed by Kawasaki and Watanabe [4] for the effective thermal stress reduction in metal and ceramic bonding, and later verified experimentally in many materials combinations [5,6]. The graded-type actuators (functionally graded actuators) are therefore expected to be more reliable than the directly bonded ones. Zhu and Meng [7] and Kouvatov et al. [8] have reported functionally graded bimorph actuators in which piezoelectric property is graded to reduce stress concentration near the interface generated by the large strain difference between two plates of the bimorph. In addition to the stress due to actuating deflection, we must take into account the thermal stress that will be induced during processing of the graded bimorph actuators. Fortunately, this thermal stress is substantially suppressed in the graded structure [4,5].

To design the functionally graded piezoelectric actuators with enhanced deflection property and mechanical reliability, it is necessary to determine the optimum composition

* Corresponding author. Tel.: +81-22-217-7355; fax: +81-22-217-7374.
E-mail address: jf-li@material.tohoku.ac.jp (J.-F. Li).

1468-6996/02/$ - see front matter
PII: S1468-6996(02)00017-7

profile that will give large deflection and low stress. The optimization in this case has been usually performed through numerical techniques [9,10] by using compositional dependency of the pertaining material properties. Recently Almajid et al. [11] have modified the classical lamination theory (CLT) for the prediction of an optimum composition profile for functionally graded piezoelectric plates, which enables us to deal with various parameters easier.

In the present study, a mixture system of lead zirconate titanate (PZT) and Pt was chosen for the fabrication of functionally graded bimorph actuator. PZT is a common type of piezoelectric ceramic, and Pt is inert to PZT, not oxidized during sintering in air, enhancing the toughness of the actuators [12], and thus stable non-piezoelectric filler in the matrix. Another advantage of the graded structure is that the bimorph structure will be fabricated in one piece by inserting a composite electrode in the mid-plane. Analytical and numerical approaches based on the modified CLT and the finite element method (FEM), respectively, were employed to predict a deflection property and an electrically induced stress in the functionally graded and conventional bimorph actuators.

2. Foundation for design and analysis

According to Almajid et al. [11], the in-plane strain vector at mid-plane, ε^0, and the curvature vector, κ, in an infinite piezoelectric plate with n laminae along z-axis as illustrated in Fig. 1, are expressed as (see Appendix A)

$$\begin{bmatrix} \varepsilon^0 \\ \kappa \end{bmatrix} = \begin{bmatrix} A & B \\ B & D \end{bmatrix}^{-1} \begin{bmatrix} N^{\mathrm{E}} \\ M^{\mathrm{E}} \end{bmatrix} \tag{1}$$

where A, B, D, N^{E} and M^{E} are the in-plane stiffness, coupling stiffness, flexural stiffness, electrical forces and electric moment matrices, respectively, and written as

$$[A, B, D] = \sum_{i=1}^{n} \int_{h_{i-1}}^{h_i} [\bar{Q}]_i (\mathrm{d}z, z\,\mathrm{d}z, z^2\,\mathrm{d}z) \tag{2}$$

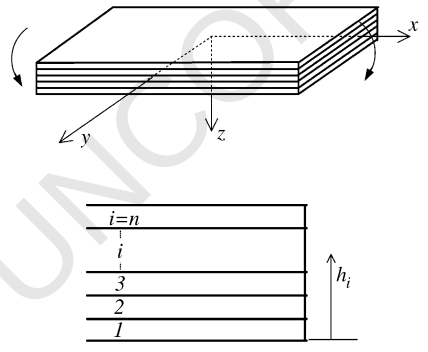

Fig. 1. Lamination model for compositionally graded piezoelectric actuation.

$$[N, M]^{\mathrm{E}} = \sum_{i=1}^{n} \int_{h_{i-1}}^{h_i} [\bar{e}]_i \{E\}_i (\mathrm{d}z, z\,\mathrm{d}z) \tag{3}$$

where h_i is the distance from bottom of the laminated plate to top of the ith lamina. It is noted that $\bar{Q}$ and $\bar{e}$ are the matrix components of the reduced stiffness constant and reduced piezoelectric constant, respectively, which are modified from material property matrices with the assumption of plane stress, and are given by

$$\bar{Q}_{ab} = C_{ab} - \frac{C_{a3}}{C_{33}} C_{b3}$$

$$\bar{e}_{ab} = \frac{C_{b3}}{C_{33}} e_{33} - e_{ab} \tag{4}$$

where C_{ab} and e_{ab} are the elastic stiffness and piezoelectric constant, and then the subscripts are given in the well-known Voigt two-index notation.

We have further derived the expression for the electric field for each lamina, E, in Eq. (3) by using a multiplayer capacitor model [12]. It is assumed that the whole laminated plate is a series condenser circuit. Whole voltage in the z-direction, V_t, is given as a sum of voltage of each lamina, V_i

$$V_t = \sum_{i=1}^{n} V_i = Q \sum_{i=1}^{n} \frac{1}{C_i} \tag{5}$$

where Q is the charge, and C_i is the capacitance of the ith lamina and expressed as

$$C_i = \frac{\varepsilon_i}{d_i} = \frac{\varepsilon_i}{h_i - h_{i-1}} \tag{6}$$

where ε_i and d_i are the dielectric constant and thickness of each lamina. Substituting Eq. (6) into Eq. (5) yields

$$Q = \frac{V_t}{\sum_{i=1}^{n} \dfrac{h_i - h_{i-1}}{\varepsilon_i}} \tag{7}$$

Thus, the electric field in each lamina is obtained by using Eqs. (6) and (7) as follows:

$$E_i = \frac{V_i}{d_i} = \frac{Q}{d_i C_i} = \frac{V_t}{\varepsilon_l \sum_{i=1}^{n} \dfrac{h_i - h_{i-1}}{\varepsilon_i}} \tag{8}$$

This equation indicates that an applied electric field in each layer depends on a ratio of dielectric constant among each layer. It means that not only the gradient of piezoelectric constant but also dielectric constant significantly affects the deflection property. The curvature of deflection, κ, is easily calculated if the elastic stiffness, piezoelectric constant, dielectric constant and thickness of each lamina and the voltage applied to whole of the specimen are known.

The in-plane stress at any distance, z is given by

$$\sigma_x = \Pi_i z \kappa_x - \rho_i E_i \tag{9}$$

Table 1
Layer thickness for the compositionally graded and directly bonded bimorph actuators

	Thickness of PZT/Pt layers (mm)			
	Electrode, 30 vol% Pt	Layer 1, 20 vol% Pt	Layer 2, 10 vol% Pt	Layer 3, 0 vol% Pt
$m = 0.5$	0.20	0.50	0.30	0.10
$m = 1.0$	0.20	0.30	0.30	0.30
$m = 2.0$	0.20	0.16	0.22	0.52
Directly bonded	0.20	–	–	0.90

where

$$\Pi = \left(C_{11} - C_{11}^2/C_{33}\right) - \frac{\left(C_{12} - C_{13}^2/C_{33}\right)^2}{\left(C_{11} - C_{13}^2/C_{33}\right)},$$
$$\rho = \left[\frac{\left(C_{12} - C_{13}^2/C_{33}\right)}{\left(C_{11} - C_{13}^2/C_{33}\right)} - 1\right]\left(\frac{C_{13}}{C_{33}}e_{33} - e_{13}\right) \quad (10)$$

3. Model for the graded bimorph actuator

Fig. 2 shows layer configuration of functionally graded bimorph actuator, in which two graded layers are symmetrically arranged with respect to the center electrode layer. The composition distribution in the upper and lower halves is expressed by Eq. (11)

$$\frac{C_l + \Delta C}{C_{\max} + \Delta C} = \left(\frac{x_l}{d}\right)^m \quad (11)$$

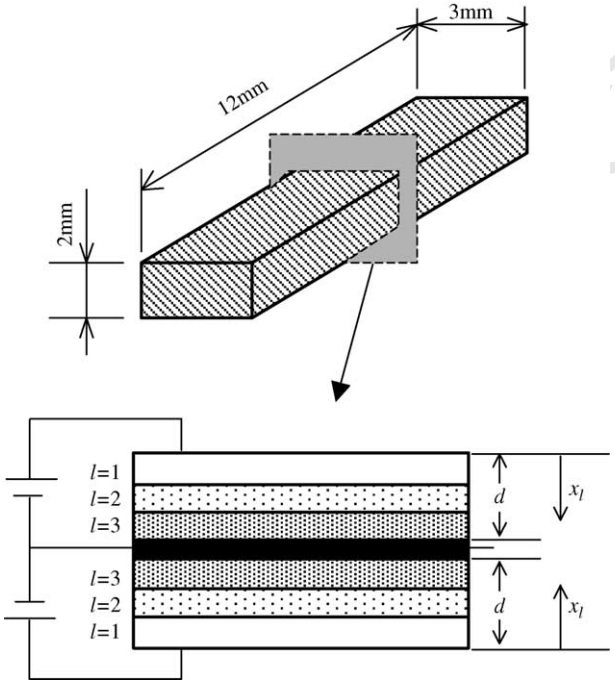

Fig. 2. Dimensions of the bimorph actuator and the cross-sectional lamination model.

where x_l is the distance from the surface to the inward face of the lth layer, as shown in Fig. 2, and C_l is the volume fraction of Pt in the lth layer. $C_{\max}$ is the maximum volume fraction of Pt in the graded layers, and ΔC is the increment of volume fraction of Pt, being equal to 0.1 in the present study. The compositional profile is characterized by the exponent m of Eq. (11). For the design of the optimum compositional profile and actual fabrication of the graded bimorph, we made a choice of a configuration of two graded layers with stepwise changed compositions arranged symmetrically with respect to the center electrode layer. The upper and lower halves have, respectively, three layers with PSZ-0, 10 and 20 vol% Pt. The center layer has a composition of PSZ-30 vol% Pt and is electrically conductive as has been reported in the previous paper [12]. The thickness of the center electrode layer (30 vol% Pt) was kept constant to be 0.20 mm. The whole configuration of the present bimorph actuators is given in Table 1, according to m values. Table 2 shows the composition dependences of the density, and elastic and piezoelectric constants [12,13], which are necessary for the calculation of the deflection and in-plane stress.

4. Assessment by FEM

The in-plane stress and curvature of deflection were also numerically calculated by FEM in order to check the validity of the lamination theory. The commercial FEM software for an elastic–electric field coupling problem (ANSYS), was used for the calculation. The FEM analysis was

Table 2
Density, elastic and piezoelectric constants for the PZT/Pt composites [12,13]

	PZT	PZT/10% Pt	PZT/20% Pt	PZT/30% Pt
ρ (kg/m^3)	790	920	1050	1187
C_{11} (GPa)	146	139	164	197
C_{12} (GPa)	95.4	87.2	108	74.3
C_{13} (GPa)	94.3	90.1	101	74.3
C_{33} (GPa)	128	134	145	197
C_{66} (GPa)	25.3	25.7	28.0	28.4
e_{31} (C/m^2)	−3.94	−3.08	−0.75	Conductive
e_{33} (C/m^2)	17.5	17.6	17.5	Conductive
$\varepsilon_{33}/\varepsilon_0$	1654	1959	2995	Conductive

performed on 2D cantilever beam model for graded and non-graded bimorphs of which dimensions are shown in Fig. 2. The boundary conditions and applied voltage were given according to the experimental conditions. The number of mesh was 15,000 in every model, and the data listed in Tables 1 and 2 were used for the calculation.

5. Experimental procedures

The fabrication procedures of the laminated bimorph actuators are described as follows. The starting materials were commercially available PZT powder (average particle size: 0.97 μm) and platinum powder (average particle size: 3.02 μm). The two powders were mixed using an agate mortar and pestle with a small amount of PVA binder. The Pt contents of the powder mixtures were 0, 10, 20, and 30 vol% for the graded layers and the electrode layer. The mixtures were stacked layer by layer into a steel die of 24 mm in inner diameter according to the design shown in Table 1, then pressed at 100 MPa, and subsequently cold isostatically pressed at 200 MPa to eliminate a possible inhomogeneity of the density in the compacts. The pressed pellets were sintered 1 h in an excess-PbO atmosphere at 1473 K, in a covered alumina (99.9% purity) crucible. The directly bonded bimorph actuator composed of two PZT layers bonded by the PZT/30 vol% Pt layer were prepared by the same procedure as described earlier. The formed specimens were cut to beams with dimensions of $12 \times 3 \times 2$ mm^3 as already shown in Fig. 2.

The microstructures of the samples were inspected by scanning electron microscopy (SEM). The thickness of each layer was measured using an image analyzer installed with an optical microscope. Silver paste was printed on both surfaces of the specimens and baked at 973 K to form the terminal electrodes. Then, the specimens were polarized under an electric field of 1 kV mm^{-1} for 30 min in a bath of silicone oil heated at 393 K. Conductive wires were attached to both the surfaces and the edge of the inner electrode by using a conductive resin. The bending deflection of the specimen was measured in a voltage range of 100–500 V by the strain gage method. The strain gages were mounted along the longitudinal direction at the center portion of the top and bottom surfaces. The voltages were supplied to both the surfaces by a DC power stabilizer, as shown in Fig. 2. The following geometrical relation converted the strain values on both the surfaces to the bending curvature of the bimorph

$$\kappa = \frac{1}{R} = \left(1 - \frac{\varepsilon_1 - \varepsilon_2}{1 + \varepsilon_1}\right) d_t^{-1} \tag{12}$$

where R and d_t are the radius of curvature and the thickness of actuator, respectively, ε_1 and ε_2 are the strain values of the expanding side and shrinking side, respectively, and their absolute values should theoretically be identical to each other.

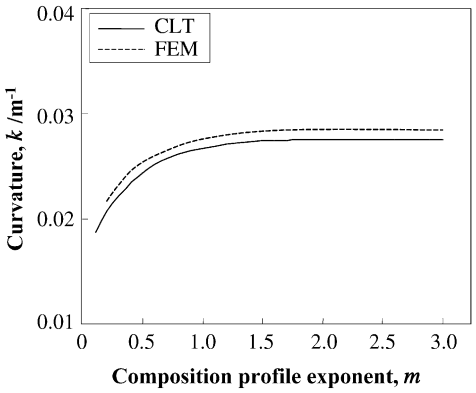

Fig. 3. Curvature versus composition profile exponent, m, for the compositionally graded bimorph actuator, as predicted by the lamination theory (CLT) and FEM. The values for the non-graded bimorph are 0.027 and 0.029 m^{-1} by CLT and FEM, respectively.

6. Results

6.1. Theoretical predictions

Fig. 3 shows the relation between the curvature and the composition profile exponent, m, both for predictions and experimental data. Let us first see the prediction curves by the lamination theory and FEM calculation. The latter gave slightly larger values, but considering the simple assumptions made in both the calculations, the agreement of the two predictions is quite well, which will justify the present analytical approach. With increase in the composition exponent the predicted values increase and approach constant values, which agree with those predicted for directly bonded bimorph. It is to be noted that at the m value of around 1.0 (linear composition profile) the curves are seen to reach a constant. The present theoretical predictions suggest the most simple composition control, that is, linear control is appropriate for the optimum design of the graded bimorph actuator.

Fig. 4 shows the FEM contours for the deflection-induced stress, σ_x, which is parallel to the interface, for the conventional (non-graded) and graded bimorphs with an applied

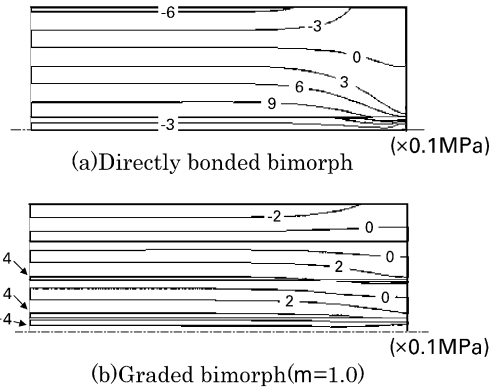

Fig. 4. Deflection-induced stresses for the upper half of the non-graded and graded bimorphs.

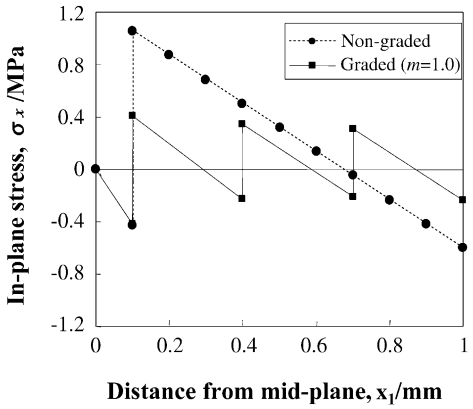

Fig. 5. In-plane stress, σ_x, versus distance from the mid-plane, x_l, for the non-graded and graded bimorphs as predicted by the lamination theory.

voltage of 100 V. The σ_x, which is a main cause for the failure of the bimorph [8,11], is generally concentrated near the interface between each layer. The stress level in the graded bimorph is much lower than that in the directly bonded one. The largest stress in the graded plate found at the interface between the electrode and 20 vol% Pt layer is less than half of the one in the conventional bimorph. Fig. 5 shows the σ_x distribution obtained by the lamination theory, which clearly shows the stress concentration and sharp stress change at the interfaces. It is confirmed here that the stress peak values are approximately in agreement with those obtained by the FEM calculation, which will also justify the present analytical approach. Fig. 6, on the other hand, shows predicted diagrams for the interfacial maximum stress versus composition profile exponent, m, although the two curves, predicted by analytical and numerical approaches, do not coincide in magnitude, they have a similar feature, and exhibit a minimum at m value of around 1.0. This means that linear composition profile will give the least stress generation. At this optimum m value graded bimorph receives approximately 50% reduction in the deflection-induced stress compared to the conventional bimorph. Note that the stress values in the present calculations are smaller than those for 3D model because the 2D model does not take into account the edge effect on xy-plane.

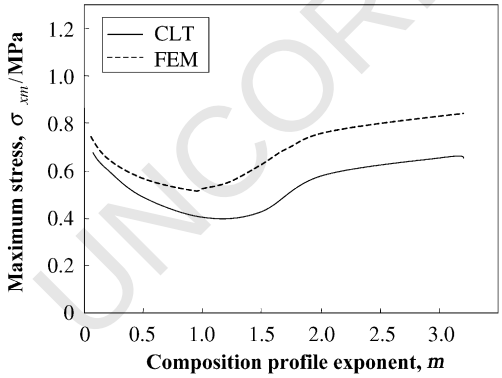

Fig. 6. Calculated maximum σ_x stress for the FGM actuators with various composition profile exponents.

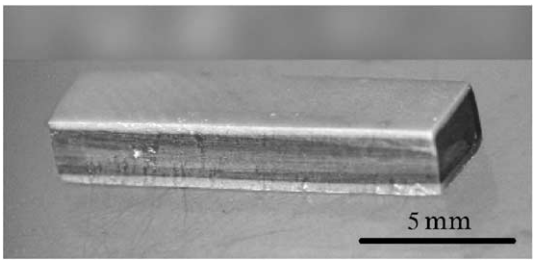

Fig. 7. Overview of the graded bimorph actuator with a linear composition profile ($m = 1.0$).

6.2. Experimental observations

Figs. 7 and 8 show the overall view and the cross-section, respectively, of the graded bimorph specimen with linear composition profile ($m = 1.0$). All the graded specimens prepared in the present investigation were inspected to have no cracks or warp. The interfaces between individual layers are seen on the micrograph to be sinter-bonded straight and parallel to the specimen surface. By the image analysis made on the micro-cross-section, the upper and lower halves are symmetrical with respect to the center electrode, and the deviation of the thickness from the designed value of each layer (Table 1) is within 50 μm. The microstructures of the individual layers are shown in Fig. 9. The gray and the white phases in these images are PZT matrix and Pt particles, respectively. No reacted zone is seen between PZT and Pt phases. The outermost PZT layer has grain sizes of 1–5 μm. Some grains were removed during polishing and their traces are seen as voids. On the other hand, the PZT/Pt composite layers have spheroidal Pt particles, the sizes of which are hundreds of nanometers to several tens of a micrometer, uniformly dispersed in the PZT matrix. The grain size of these composite microstructures ranges from 1 to 3 μm, being much smaller than that for the monolithic PZT layer. According to our previous studies [12,13], the PZT/Pt composites containing more

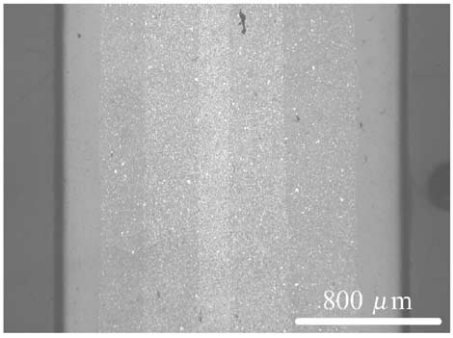

Fig. 8. Cross-section of the graded bimorph actuator with a linear composition profile ($m = 1.0$).

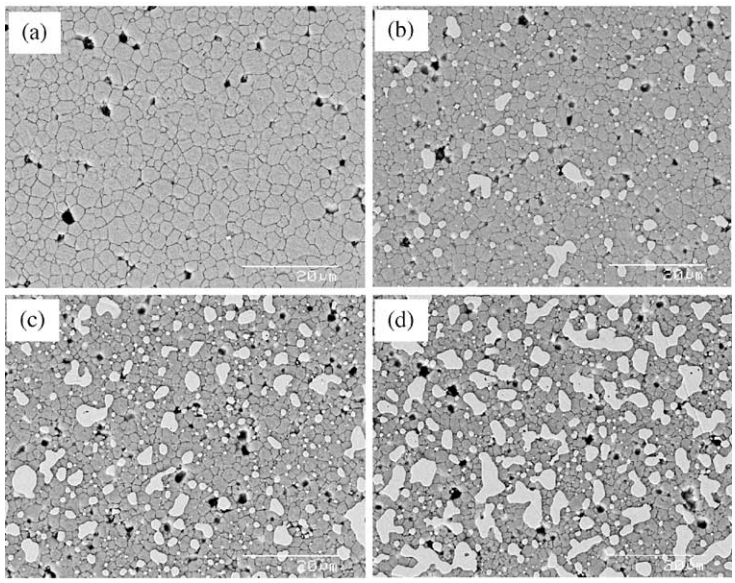

Fig. 9. SEM micrographs of each layer shown in Fig. 8. (a) PZT/0% Pt, (b) PZT/10% Pt, (c) PZT/20% Pt and (d) PZT/30% Pt.

than 20 vol% Pt have 2–3 times as high fracture strength as pure PZT owing to the bridging effect and to the fine and uniform microstructures [14]. The 30% Pt composite is electrically conductive because of the 3D connection of Pt phases [12], and will serve as an inner electrode.

It was confirmed that as the applied voltage increases, the strains on both sides of the bimorph increases and bending deflection appears. The magnitude of the strains is roughly proportional to the applied voltage. The curvature of deflection, κ, converted from both the strains according to Eq. (11), is plotted against the applied voltage for $m = 1$, as shown in Fig. 10, along with the theoretical line predicted by the lamination theory. A linear relation is found between the curvature and the applied voltage, and this linearity is valid for all m values. The theoretical line gives smaller values than that of the experimental, however, the difference is rather small.

Fig. 11 shows the experimental result for the curvature versus composition profile exponent, m. The analytical curve is also shown in the diagram. The experimentally observed curvature increases with an increase in the exponent, but shows higher values at larger m values than predicted by the lamination theory. It is to be noted that at the m value of 2.0 the curvature of the graded bimorph exhibits a curvature of $0.031\ m^{-1}$, which is significantly larger than that of the conventional (non-graded) bimorph.

7. Discussion

The compositionally graded bimorph has been verified to exhibit a deflection characteristic comparable to the directly bonded bimorph. The deflection-induced strain for this graded bimorph would not exceed one-half of that for the conventional one as estimated by the analytical and numerical calculations. The low stress will assure the graded bimorph of a long life as an oscillating actuator with high frequency. In the present mixing condition of PZT and Pt, the linear composition profile will give an optimum design for a satisfactory deflection characteristic and low stress generation. It has been shown in the present study that the lamination theory gives a good estimation of the deflection and the induced stress for the graded bimorphs. It should be mentioned that although the FEM will give a more accurate estimation for the deflection behaviors than the lamination theory, the latter is more advantageous in the design of the graded bimorphs, because it is an analytical method and the calculation is much easier than the numerical method.

Here the difference in the curvature between the predicted and the observed, as shown in Fig. 11, will be discussed. The observed curvature of the graded bimorph actuator with a

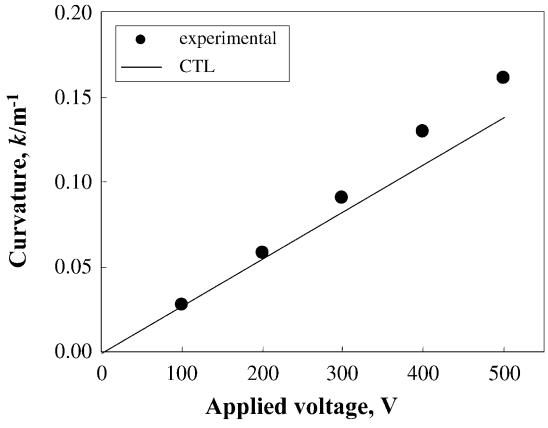

Fig. 10. Relationships between an applied voltage and curvature in the graded actuator with a linear composition profile ($m = 1.0$). The straight line is predicted by the lamination theory (CLT) and the circles are experimental data.

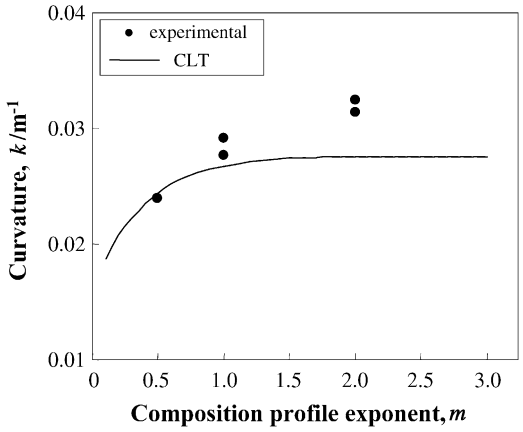

Fig. 11. Predicted and measured curvature values of the graded bimorphs as a function of composition profile exponent, *m*. The line is predicted by the lamination theory (CLT) and the circles are experimental data. The measured and predicted curvature values for the non-graded actuator are 0.028 and 0.027 m^{-1}.

composition profile exponent, *m*, of 2.0 exceeds the predicted value. Two reasons are to be postulated for this discrepancy: one is thermal residual stress induced during processing, and the other is non-uniform poling. The former was experimentally checked by measuring the deflection of the conventional thermal-stress-free bimorph directly bonded with an organic adhesive. We did not find any difference between the sinter-bonded and adhesive-bonded bimorph. Actually the curvature for the adhesive-bonded bimorph was measured to be 0.028 m^{-1}, which was exactly identical to that of the sinter-bonded one that should have the largest residual stress generation during processing. We have therefore concluded that the thermal residual stress has no effect on the deflection behavior of the bimorph actuator. The second point is related to the voltage distribution during poling graded samples. As has been described in the theoretical foundation, the laminated bimorph with composition grading can be considered to form a series capacitor circuit, and then the distribution of the voltage was taken into account in the lamination theory as given by Eq. (8). Such a voltage sharing would work during poling. For example, when the graded bimorph with $m = 1.0$ is poled at 1 kV/mm, the PZT/0, 10 and 20% Pt layer will receive the electric fields of 1.39, 1.18 and 0.77 kV/mm, respectively, according to Eq. (8). This means that every layer in the graded bimorph is poled under different voltages and the poling-voltage dependent properties are not strictly equal to the properties in Table 2 used in the present calculations. Especially, it is very likely that the PZT/20% Pt layer was not poled enough and had lower piezoelectric constants than expected, because it has been reported that the coercive force of the PZT/Pt composite is more than 0.8 kV/mm [15]. We tentatively made a calculation for the curvature by the lamination theory on the assumption that the piezoelectric constants of PZT/20% Pt layer were zero, which meant that this layer had not been poled due to insufficient voltage. Similar *m*-dependency to the experimentally observed one was obtained by this calculation. We must take into account such an effect for a better design of the graded bimorph actuator. Further investigation is under way on the voltage distribution during poling of the graded bimorph.

8. Conclusion

1. The compositionally graded piezoelectric bimorph actuator in the PZT/Pt mixing system exhibits a better deflection property than the non-graded bimorphs.
2. The modified lamination theory is well applied to design the compositionally graded piezoelectric bimorph actuator with an optimum composition profile and the least deflection-induced stress generation.
3. For the present materials and processing conditions the linear composition profile gives the lowest stress generation and a bending deflection comparable to that of the conventional bimorphs.

Appendix A. The modified classical lamination theory for an infinite FGM piezoelectric plate

Almajid et al. [11] modified CLT by introducing the constitutive equations for the piezoelectric materials to adapt to the graded piezoelectric multi-laminated plates. It is assumed the model is a state of plane stress in the thickness direction, which is defined as *z*-axis as shown in Fig. 2, and based on the Kirchhoff–Love hypotheses for a thin plate, i.e. $\sigma_z = \sigma_{xy} = \sigma_{yz} = 0$. The constitutive equation f or the piezoelectric material in the absence of temperature effect is given by

$$\{\sigma\} = [\bar{Q}]\{\varepsilon\} - [\bar{e}]\{E\} \tag{A1}$$

where σ, ε and E are the stress, strain and electric field vectors, $\bar{Q}$ and $\bar{e}$ are the reduced elastic stiffness and reduced piezoelectric coefficient matrices given by Eq. (4). The relationship between an in-plane stress and strain at any distance, *z*, without considering piezoelectric effect is written as

$$\{\varepsilon\} = \{\varepsilon^0\} + z\{\kappa\} \tag{A2}$$

where ε^0 and κ are the in-plane strain vector at mid-plane and the curvature vector. Substituting Eq. (A2) into Eq. (A1) gives the following:

$$\{\sigma\} = [\bar{Q}](\{\varepsilon^0\} + z\{\kappa\}) - [\bar{e}]\{E\} \tag{A3}$$

Here, when the state of plane stress with $\sigma_y = \sigma_{xy} = 0$ is additionally assumed, in-plane stress σ_x can be obtained as Eq. (9), in which the material constants such as Π and ρ are reduced from $\bar{Q}$ and $\bar{e}$ based on the assumption of 1D beam theory model.

On the other hand, the resultant in-plane forces and

bending moments are defined by

$$\{N, M\} = \sum_{l=1}^{k} \int_{h_{l-1}}^{h_l} \{\sigma\}_l (\mathrm{d}z, z\,\mathrm{d}z) \tag{A4}$$

Eq. (A4) can be rewritten in the following form by working out the integration by using Eq. (A3):

$$\begin{bmatrix} N \\ M \end{bmatrix} = \begin{bmatrix} A & B \\ B & D \end{bmatrix} \begin{Bmatrix} \varepsilon^0 \\ \kappa \end{Bmatrix} - \begin{bmatrix} N^{\mathrm{E}} \\ M^{\mathrm{E}} \end{bmatrix} \tag{A5}$$

where A, B, C and D are presented in Eq. (2). Eq. (A5) can be rewritten as Eq. (1).

References

[1] Y. Yee, H.-J. Nam, S.-H. Lee, J.U. Bu, J.-W. Lee, PZT actuate micromirror for fine-tracking mechanism of high-density optical data storage, Sens. Actuators A89 (2001) 166–173.

[2] S. Wang, J.-F. Li, K. Wakabayashi, M. Esashi, R. Watanabe, Lost silicon mold process for PZT microstructure, Adv. Mater. 10 (1999) 874–876.

[3] J. Tani, Intelligent materials and structures, Trans. JSME (C) 60 (1994) 28–35.

[4] A. Kawasaki, R. Watanabe, Finite element analysis of thermal stress of the metal/ceramic multi-layer composites with controlled compositional gradient, J. Jpn Inst. Metal 51 (1987) 525–529.

[5] A. Kawasaki, R. Watanabe, Microstructural designing and fabrication of disk shaped functionally gradient material by powder metallurgy, J. Jpn. Soc. Powder Powder Metall. 37 (1990) 253–258.

[6] T. Hirai, Functional gradient materials, in: R.J. Brook (Ed.), Processing of Ceramics, Part 2, Materials Science and Technology, vol. 17B, VCH, Weinheim, 1996, pp. 293–341.

[7] X. Zhu, Z. Meng, Operational principle, fabrication and displacement characteristics of a functionally gradient piezoelectric ceramic actuator, Sens. Actuators A48 (1995) 169–176.

[8] A. Kouvatov, R. Steihausen, W. Seifert, T. Hauke, H.T. Langhammer, H. Beige, H. Abicht, Comparison between bimorphic and polymorphic bending devices, J. Eur. Ceram. Soc. 19 (1999) 1153–1156.

[9] B.L. Wang, N. Noda, Design of a smart functionally graded thermopiezoelectric composite structure, Smart Mater. Struct. 10 (2001) 189–193.

[10] J.-F. Li, M. Ono, M. Taya, R. Watanabe, Fabrication and evaluation of porosity-graded piezoceramic actuators, Ceramic Transaction (Proceedings of FGM2000), American Ceramic Society, 2002 in press.

[11] A. Almajid, M. Taya, S. Hudnut, Analysis of out-plane displacement and stress field in a piezoelectric plate with functionally graded microstructure, Int. J. Solids Struct. 38 (2001) 3377–3391.

[12] J.-F. Li, K. Takagi, N. Terakubo, R. Watanabe, Electrical and mechanical properties of piezoelectric ceramic/metal composites in the $Pb(Zr,Ti)_3$/Pt system, Appl. Phys. Lett. 79 (2001) 2441–2443.

[13] N. Terakubo, J.-F. Li, R. Watanabe, Fabrication of functionally graded PZT/Pt piezoelectric actuators, J. Jpn. Soc. Powder Powder Metall. 47 (2000) 1216–1220.

[14] H.J. Hwang, M. Yasuoka, M. Sando, M. Toriyama, Fabrication, sinterability, and mechanical properties of lead zirconate titanate/silver composite, J. Am. Ceram. Soc. 82 (1999) 2417–2422.

[15] N. Duan, J.E. ten Elshof, H. Verweij, G. Greuel, Dannapple, Enhancement of dielectric and ferroelectric properties by addition of Pt particles to a lead zirconate titanate matrix, Appl. Phys. Lett. 77 (2000) 3263–3265.